Biochemical and Biophysical Research Communications 600 (2022) 117–122

Contents lists available at ScienceDirect

Biochemical and Biophysical Research Communications

journal homepage: www.elsevier.com/locate/ybbrc

Structure-guided rational design of the *Geobacillus thermoglucosidasius* feruloyl esterase GthFAE to improve its thermostability

Wendi Yang, Lifang Sun, Panpan Dong, Yayu Chen, Hong Zhang, Xiaojin Huang, Linjiao Wu, Leiqing Chen, Dindin Jing, Yunkun Wu*

Provincial University Key Laboratory of Cellular Stress Response and Metabolic Regulation, College of Life Science, Fujian Normal University, Fuzhou, 350117, China

ARTICLE INFO

Article history:
Received 13 February 2022
Accepted 18 February 2022
Available online 20 February 2022

Keywords:
Feruloyl esterase
Structure
Rational design
Thermostability
Active center

ABSTRACT

Feruloyl esterases are indispensable biocatalysts catalyzing the cleavage of ester bonds between polysaccharides and their hydroxycinnamoyl cross-links. GthFAE from *Geobacillus thermoglucosidasius* was identified as a thermophilic alkaline feruloyl esterase with potential applications in paper manufacturing. To improve the enzymatic properties rationally and efficiently, the structure of GthFAE was solved at 1.9 Å, revealing a core domain of classical α/β hydrolase fold and an inserted α/β cap domain. *In silico* analysis based on it helped us to investigate whether the residues at the active center have positive effects on the stability, and how. Several site-directed mutations were conducted, of which substitutions at residues T41 and T150 apparently improved the thermostability. The combination mutant T41N/T150R exhibited an optimal temperature of 65 °C, a 6.4 °C higher T_m compared to wild type by 80 °C, and a 35-fold longer in half-life (201 min) at 70 °C. Molecular dynamics simulations further illustrated that the structure of T41N/T150R was more stable than the wild type and T150R stabilized the cap domain by introducing salt bridges to the region with E154 and D164. This study not only highlighted residues within the active center on their thermostability improving effects, but also contributed to the prospective industrial application of GthFAE.

1. Introduction

Feruloyl esterases (ferulic acid esterases, FAEs; EC 3.1.1.73), namely cinnamoyl esterases, are members of the α/β hydrolase superfamily that can hydrolyze ester bonds between polysaccharides and their hydroxycinnamoyl cross-links in hemicellulose of plant cell walls [1]. Assisting the breakdown of plant cell walls with ferulic acid or other hydroxycinnamic acids released, FAEs have variety biotechnological applications as potential biocatalysts in pharmaceutical biosynthesis, food and feed industries, paper production, biomass degradation and production of renewable fuels [1,2]. Hundreds of FAEs have been identified from bacteria, fungi and plants, since the first purification and characterization in 1990s, and accelerating scientific discoveries were achieved in recent years [3–7]. The enzymes from different sources present a broad range of structural, biochemical and enzymatic characteristics that FAEs have their optimum temperature at 50 °C and pH at 6.5 according to relative frequencies and medians [1]. Nevertheless, seldom of them perform well in alkaline conditions or temperatures higher than 60 °C, which may not meet the demand for industrial applications, since, for example, the bleaching stage for paper manufacturing is conducted in strong alkaline and high temperature conditions.

Enzymes are attractive and competitive alternatives to chemical catalysts, but only a minority of them were industrialized [8]. Thermostability is one of the most significant measurements for industrial enzyme selection. Thermophilic enzymes enable high working temperatures that adapt to the harsh conditions of industrial processes, reduce the risks of microbial contamination, improve the reusability and determine the economic feasibility [9]. Thermostable enzymes are mainly discovered by two ways: identified from thermophilic bacteria and enzyme engineering including random mutagenesis, directed evolution, rational design

* Corresponding author.
E-mail address: wuyk@fjnu.edu.cn (Y. Wu).

https://doi.org/10.1016/j.bbrc.2022.02.074
0006-291X/

and semi-rational design [10–14]. Among these engineering strategies, computer-aided rational design guided by protein structure, would be most attractive in recent years, due to its efficiency and cost-saving, with more computational tools and structural information available.

Previous study has purified and characterized a thermophilic alkaline feruloyl esterase, GthFAE, from *Geobacillus thermoglucosidasius* (*Parageobacillus thermoglucosidasius*) DSM 2542^T in 2019 [3]. *G. thermoglucosidasius*, acting as an important source of industrial enzymes, is a thermophilic gram-positive bacterium first isolated from soil in 1983, with growth temperatures from 42 °C to 69 °C and an initial pH of 6.5–8.5 [15]. GthFAE was found to exhibit high stability and optimum pH with optimal activity at 50 °C and pH of 8.5 [3]. The FAE was superior to most of its counterparts that could retain more than 80% of its enzymatic activity after 8 h in 40–60 °C, and 90% of activity in alkaline environments after 120 min [1,3]. Besides, the enzyme could be expressed heterologously in *E. coli*, and purified by ion-exchange column chromatography or affinity column chromatography, with the specific activities on methyl and ethyl ferulate 161.7 ± 6.94 U/mg and 19.02 ± 2.36 U/mg, respectively [3]. Accordingly, GthFAE was suggested to be a potential industrial feruloyl esterase, especially in the paper manufacturing by its thermostability, alkali-resistance, PH stability, acceptable enzymatic activity and suitability for scale-up production. Only a few structures of bacterial FAEs had been solved, therefore, to further enhance its advantages in thermostability, a crystallographic study was necessary for GthFAE engineering by providing theoretical foundation and preliminary information. Site-directed mutagenesis was conducted on the residues around the active center with improved thermostability observed, and *in silico* analysis explained the possible molecular mechanisms.

2. Materials and methods

2.1. Strains, plasmids and chemical reagents

The gene of GthFAE (GenBank: MG834533.1) was codon-optimized, synthesized, cloned into plasmids pET28a and modified pET32a, and expressed in *E. coli* BL21 (DE3). The GthFAE-pET32a construct ligated GthFAE with a thioredoxin (Trx) and an N-terminal 6*His tag by a tobacco etch virus (TEV) cleavage site. All chemicals were obtained commercially.

2.2. Heterologous expression and purification

The GthFAE-pET32a construct was consisted of residues 2–252 and purified for crystallization, while the full-length GthFAE and its mutants were constructed on pET28a for enzyme engineering. The expression and purification were performed as described in our previous study [16]. Both constructs were purified by the Ni^{2+}-NTA resin affinity column (GE Healthcare, USA), while additional removal of Trx-His-tag by TEV protease and Ni^{2+}-NTA affinity chromatography was required for pET32a construct before gel filtration chromatography by HiLoad 16/600 Superdex 200 pg column (GE Healthcare, USA). The molecular weight and purity of recombinant GthFAE were analyzed by 15% SDS-PAGE.

2.3. Crystallization, X-ray data collection and structure determination

Hundreds of crystallization conditions were screened by the sitting-drop vapor-diffusion method at 16 °C. The crystals were observed in a variety of PEG-based conditions, and fortunately, reached diffraction quality in 0.1 M Tris-HCl pH 7.0, 20% PEG1000 within one week. Then crystals were flash-frozen in liquid nitrogen with additional PEG400 as the cryoprotectant. X-ray diffraction data sets were collected at beamline BL17B1 of the Shanghai Synchrotron Radiation Facility (SSRF, Shanghai, China). Data were processed and scaled with HKL-2000, and the structure was determined by molecular replacement using Phaser with the *Lactobacillus johnsonii* Cinnamoyl Esterase LJ0536 apo structure (PDB code: 3PF8) as a starting model [17–19]. Moreover, model building and refinement were performed with Coot and PHENIX [20,21]. Structural figures were generated by Pymol (https://pymol.org/2/), and the coordinate files and structure factors were deposited to the Protein Data Bank with accession code 7WWH.

2.4. Characterization of enzymatic thermostability

Enzymatic activity was measured by the spectrophotometric method using *p*-nitrophenyl ferulate (*p*NPF) as substrate. The reaction was stopped by chilling in ice, and the production *p*NP was monitored at 410 nm. One unit of enzyme activity (1 U) was defined as the amount of enzyme liberating 1 μmol of *p*NP per minute under the assay conditions. The optimal temperature of GthFAE was measured from 50 °C to 80 °C at intervals of 5 °C. The half-life ($T_{1/2}$) was determined by the incubation time of GthFAE treated at 70 °C until 50% residual activity.

The melting temperature (T_m) of GthFAE was measured to detect protein unfolding by nano differential scanning fluorometry (nanoDSF, Prometheus NT.48 instrument from NanoTemper Technologies, Munich, Germany), capturing changes in intrinsic fluorescence at emission wavelengths of 330 and 350 nm. The samples were analyzed 20–95 °C with temperature slope 1 °C/min.

2.5. Site-directed mutagenesis

Computational procedures were utilized to select the site-directed mutant sites. Semi-flexible molecular docking of GthFAE with substrate *p*NPF was performed by Autodock 4.2 to recognize the active site defined as residues within 5 Å of the substrate [22]. Structure of the ligand *p*NPF was obtained from the PubChem database (https://pubchem.ncbi.nlm.nih.gov/), and the receptor was defined as chain A of GthFAE. Conservation of residues was analyzed by "https://consurf.tau.ac.il/" \o "https://consurf.tau.ac.il/" "https://consurf.tau.ac.il/" The ConSurf Server (tau.ac.il). Screening for flexible residues with high B-factors were realized by B-FITTER [23]. Furthermore, the stability of mutants was predicted by their unfolding free energy change ΔΔG values calculated by FoldX that ΔΔG<0 indicated a higher stability than wild type [24]. In the wet experiments, the full-length pET28a construct of GthFAE was considered as a template for PCR amplification of the site-directed mutagenesis. Confirmed by DNA sequencing, the mutants were expressed and purified identical with the wild type.

2.6. Molecular dynamic simulation

Molecular dynamics (MD) simulations of the protein were performed by Gromacs 2019.6 (http://www.gromacs.org/) with AMBER ff99SB-ILDN force field at 298K for 20ns mentioned in our previous study [16]. The convergence of the MD simulations on each system was monitored by the Root Mean Square Deviation (RMSD) values of the backbone atoms, and the average root mean square fluctuation (RMSF) values for residues were calculated at the last 2 ns after the systems went into equilibrium.

3. Results and discussion

3.1. Crystal structure of GthFAE

The 28 kDa recombinant GthFAE was purified to homogeneity for crystallization, and the enzyme existed as a dimer in solution according to the molecular weight analyses of SDS-PAGE and gel filtration chromatography (Fig. S1). The structure was determined at a resolution of 1.9 Å, and it belonged to the space group $P\ 1\ 2_1\ 1$ with the cell constants $a = 46.04$ Å, $b = 87.41$ Å, $c = 69.46$ Å, $\alpha = \gamma = 90°$ and $\beta = 95.97°$. The diffraction and refinement statistics were summarized in Table 1. Each asymmetric unit contained two identical molecules sharing the RMSD of 0.589 Å over Cα atoms, however, as calculated by the PDBe PISA server (https://www.ebi.ac.uk/msd-srv/prot_int/cgi-bin/piserver), the molecules did not exhibit extensive contacts with each other, indicating that, different from the status in solution, the two monomers were due to crystal packing instead of dimerization.

The structural analyses hereafter were based on monomer A, which comprised a core domain of classical α/β hydrolase fold and an inserted α/β cap domain (Fig. 1A). In the core domain, the twisted central β-sheet was made up of one antiparallel β-strand pair (β1 and β2) and six parallel β-strands (β3-β6, β9 and β10) forming a βαβ sandwich with two flanks of α-helices: α1 and α8 on one side, α2, α3 and α7 on the other. The cap domain, atop the active sites to regulate the entrance of substrates in GthFAE, was situated between β6 and β9 comprising 3 α-helices (α4-α6) and a pair of short antiparallel β-strands β7 and β8. The Dali server suggested that the closest homologue of GthFAE with known structure was chain A of LJ0536, which was exactly the starting model for molecular replacement and shared a 37% sequence identity for 95% coverage with Z-score of 36.0 and RMSD 1.4 Å [25]. Similar to LJ0536, GthFAE has two Gly-X-Ser-Gly motifs, as Gly72-Ser74-Gly76 and Gly112-Ser114-Gly116, respectively, with only Ser114 forming the conserved catalytic triad with Asp202 and His232. The catalytic triad was located in the hydrophobic pocket between the core and cap domains, and the nucleophile Ser114 was situated at the nucleophile elbow between β5 and α3. The major difference between the homologs lay in the cap domain (RMSD = 6.7 Å for Cα) with an additional pair of antiparallel β-strands in LJ0536, leading to the different performances in their specific esterase activities. Both esterases could react with substrates *p*-nitrophenyl butyrate, *p*-nitrophenyl caprylate and ethyl ferulate in previous studies, while GthFAE showed higher activities to them all, resulting from the more open catalytic pocket shaped by the cap domain [3,26].

Table 1
Data collection and refinement statistics.

Parameter	Value(s)
Data collection	
Beamline	SSRF BEAMLINE BL17B1
Wavelength (Å)	0.97854
Space group	$P\ 1\ 2_1\ 1$
Unit cell dimensions	
a, *b*, *c* (Å)	46.04, 87.41, 69.46
α, β, γ (°)	90, 95.97, 90
Resolution range (Å)	50.00–1.91 (1.94–1.91)
Completeness (%)	98.70 (94.60)
Redundancy	6.70 (6.20)
No. of reflections measured	617692
No. of unique reflections	41148
R_{merge}	0.073 (0.505)
$<I/\sigma(I)>$	5.60 (3.46)
$CC_{1/2}$	0.994 (0.905)
Wilson B-factor (Å^2)	24.80
Refinement	
R_{work}/R_{free} (%)	17.43/20.34
No. of molecules per asymmetric unit	2
Residues included	Chain A: 2-252 Chain B: 2-252
Total No. of atoms	4365
Ramachandran plot (%)	
Favored regions	95.98
Allowed regions	4.02
Outliers	0
Average B-factor, all atoms (Å^2)	32.64
PDB	7WWH

Values in parentheses refer to the highest resolution shell.

3.2. Selection of mutagenesis for thermostability improvement

The variations in the architecture of cap domains and catalytic pockets related extensively with the diversities in enzymatic substrate preferences, catalytic activities and thermostability. Although seldom residues at the catalytic pockets were selected for thermostability improvement in previous studies, there was a successful active center stabilization strategy utilized to improve the kinetic thermostability of *Candida rugosa* lipase1 by site-saturation mutagenesis. Compared to the wild type, a multi-site mutant (F344I/F434Y/F133Y/F121Y) revealed a 40-fold longer in half-life at 60 °C and a 12.7 °C increase in T_m with no decrease in activity [27]. Considering that the GthFAE residues with B-factors ranked top 20 were all situated in the cap domain not far from the catalytic pocket (Fig. 1B), attempts to improve its thermostability were focused on it.

To find the catalytic pocket for GthFAE, molecular docking study was performed to dock the substrate *p*NPF into the hydrophobic cavity of GthFAE, resulting 12 distinct conformational clusters from 300 runs. The Rank 1 cluster included conformations far more than the others, and more important, contained the one with the lowest binding energy by −8.18 kcal/mol. In the conformation, there were 19 residues within 5 Å of *p*NPF composing the catalytic pocket, however, eliminated the highly conserved residues, only 11 of them were considered as candidates for mutagenesis (Fig. 1C). According to the multiple sequence alignment for conservation analysis, asparagine appeared far more frequently at corresponding sites to residue 41 in the sequence homologs as Thr41 in GthFAE, and the situation was similar for alanine to Ile147. Moreover, Met143, Leu146, Ile147 and Thr150 were selected for mutation *in silico* by PositionScan with FoldX because their B-factors were ranked top (Table S1). Three of them, except Met143, could find mutants ΔΔG<0, which should be beneficial mutants, with, notably, Thr150 as a "hot spot" due to its 14 out of 19 mutants exhibiting negative ΔΔG values. Thr41 was located in the loop between β3 and α1 in the core domain, while Leu146, Ile147 and Thr150 were all situated on α4 in the cap domain facing the catalytic pocket. The residues were all surface-exposed. Consequently, mutagenesis was conducted to Thr41, Leu146, Ile147 and Thr150, with more attention paid on Thr150, constructing 6 mutants: T41N, L146A, I147A, T150Y, T150R and T150I.

3.3. Enzymatic thermostability characterizations for the mutants

Measurement of the thermostability properties could confirm whether the design would work with GthFAE. The enzymatic activities were measured with substrate *p*NPF for the wild type and its mutants mentioned above, and the criteria for evaluation of a mutant involved its impacts on both thermostability and activity. Different from the previous report, the optimum temperature for GthFAE was observed to be 60 °C, instead of 50 °C. L146A, I147A and T150I were not further studied, because the crude enzymic relative activities for I147A and T150I, different from their counterparts,

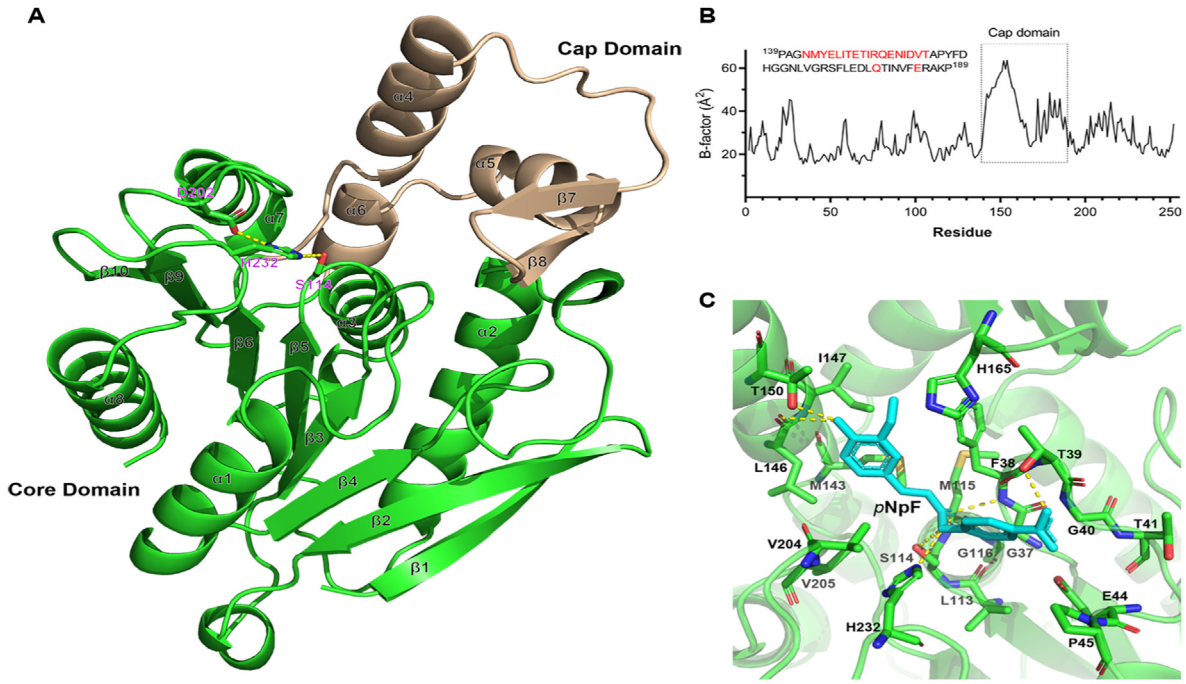

Fig. 1. Overall structure of GthFAE. **(A)** Cartoon representation of GthFAE. The structure is consisted of a core α/β hydrolase fold (colored green) and an inserted cap domain (colored wheat), with the catalytic triad S114-D202-H232 shown in sticks. **(B)** B-factors for the residues. The residues in the cap domain are listed with B-factors ranked top 20 in red. **(C)** Catalytic pocket of GthFAE and its polar contact with *p*NPF. GthFAE in green, and *p*NPF in blue. (For interpretation of the references to color in this figure legend, the reader is referred to the Web version of this article.)

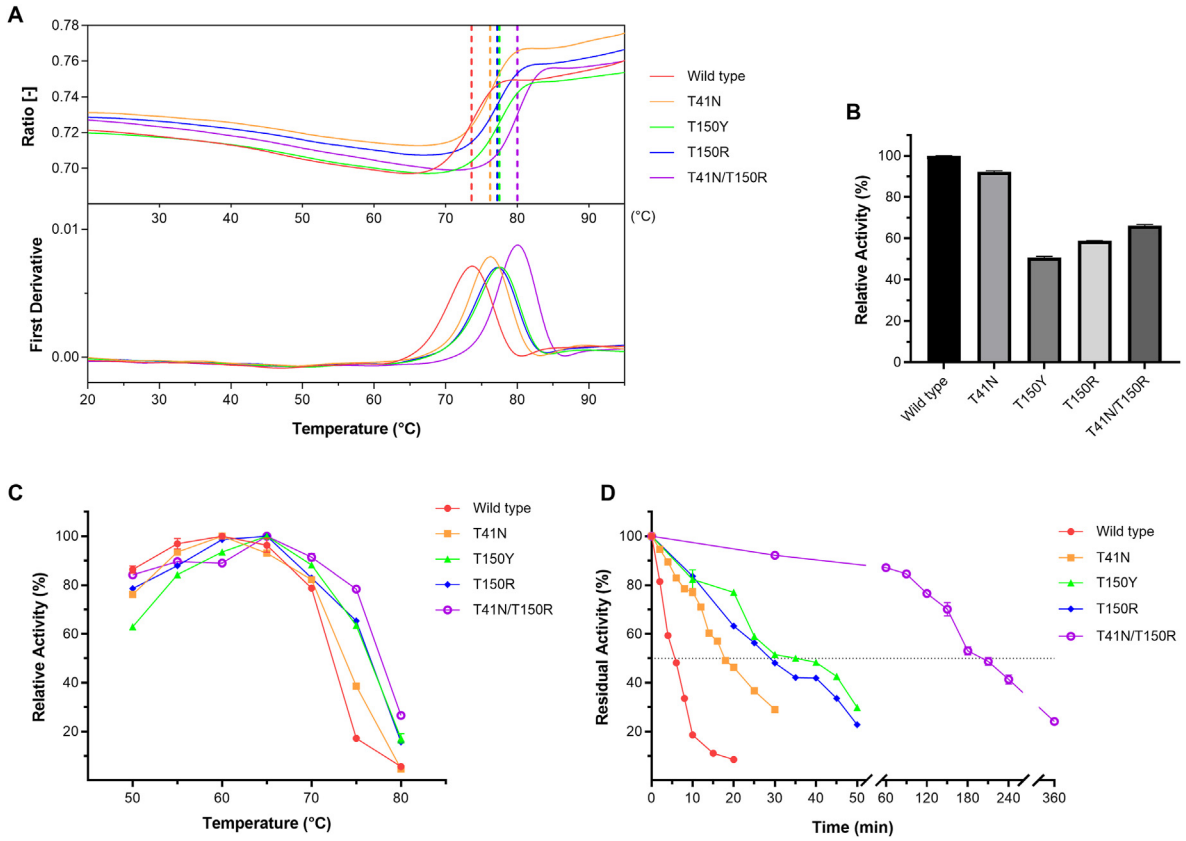

Fig. 2. Thermostability for the wild type and mutants. **(A)** Melting temperatures (T_m) determined by nanoDSF signal ratio 350 nm/330 nm and its first derivative plots in function of temperature. The T_m values for the wild type, T41N, T150Y, T150R, T41N/T150R are shown in dashed line at 73.6 °C, 76.2 °C, 77.5 °C, 77.2 °C and 80 °C respectively. **(B)** Relative activities toward *p*NPF. **(C)** Optimal temperatures. **(D)** $T_{1/2}$ determined by the residual activities at 70 °C. The data involved are mean ± SD in triplicate for each sample in **(B)**, **(C)** and **(D)**.

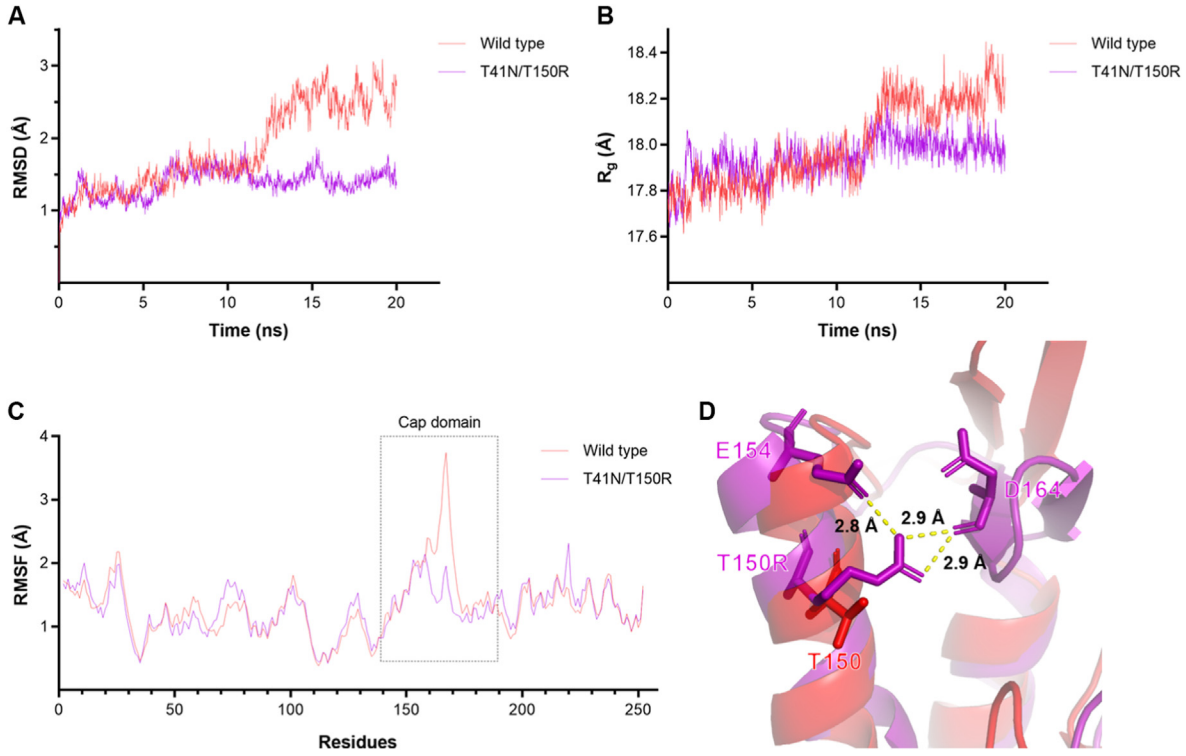

Fig. 3. MD simulations of wild type and T41N/T150R. **(A)** RMSD values of the backbone Cα atoms. **(B)** Mass-weighted R_g of the non-hydrogen atoms. **(C)** Average RMSF values of residues for the last 2 ns. **(D)** Superimposition at regions around residue 150. Wild type colored in red, and T41N/T150R in purple. Different from T150, the side chain of T150R forms salt bridges with E154 and D164. (For interpretation of the references to color in this figure legend, the reader is referred to the Web version of this article.)

were less than 50% of the wild type while, although that for L146A was 122%, the T_m value of it was lower than wild type (Fig. S2).

As shown in Fig. 2, the T_m values of T41N, T150Y and T150R mutants were 2.6 °C, 3.9 °C and 3.6 °C higher than the wild type (73.6 °C), respectively, with T150Y highest by 77.5 °C. The combining mutations could create miracles with significant increase, for instance, a 10-fold mutant of an alcohol dehydrogenase had been generated with +51 °C in T_m [13]. Since T_m values of T150Y and T150R were similar by a tiny gap of 0.3 °C, considering the higher activity of T150R, we only combined T150R to T41N forming the mutant T41N/T150R with T_m reaching 80 °C, increased by 6.4 °C. Unfortunately, contrary to their rising T_m, the enzyme activities were decreased for all the mutants, compared by relative activities at 60 °C, with T41N closest to the wild type and followed by T41N/T150R.

The enzymic activities of wild type and mutants of GthFAE were measured at various temperatures to investigate the changes in optimal temperature. The optimal temperature for T41N was 60 °C, which was consistent with recombinant GthFAE in our study. The parameters shifted to 65 °C for the other three mutants that hardly reached by FAEs in previous reports [1,3]. At 75 °C, when the wild type only remained 17% of its activity, they still exhibited high activities as more than 60%, T41N/T150R, especially, retained 78%. All of the enzymes performed high activities in a wide temperature range, with more than 80% activities at 50–65 °C for the wild type, 55–70 °C for the three single-site mutants, and 50–70 °C for the combined mutant. The residual activities of GthFAE and its mutants were measured at 70 °C. The $T_{1/2}$ of wild type was about 5.7 min, whereas, that for T41N, T150Y and T150R were roughly 18 min, 35 min and 29 min, respectively, indicating 3.1- to 6.2-fold of wild type $T_{1/2}$. T41N/T150R retained more than 50% of its initial activity after incubation for 3 h, with the $T_{1/2}$ 201 min, 35 times to wild type. It only sacrificed less than 25% activity after heating 2 h, and its residual activity for 6 h was 24%. Therefore, the mutagenesis could highly improve the thermostability, both single and combined, with the remarkable performance of T41N/T150R in high temperature.

3.4. Structural analysis of the T41N/T150R mutant

Minor modification of the protein structure can realize the thermostability enhancement by one or more strategies, such as the introduction of noncovalent or covalent bonds, increase of proline and/or decrease of glycine, reinforcement of subunit–subunit interactions, addition of glycosylation sites, truncation, cyclization and etc. We supposed that the thermostability improvement of the combination mutant in this study was a combined result of introducing salt bridge between T150R and aspartic or glutamic acid around, and improving the hydrophilic activity of the protein surface by T41N.

To investigate the molecular basis of the thermostability performance, the molecular dynamics simulations were conducted to examine the structural changes of GthFAE before and after mutation. The analyses of RMSD and radius of gyration (R_g) both indicated that the structure of T41N/T150R was more stable than the wild type with the RMSD values of the backbone Cα atoms characterizing the stability of the systems and R_g representing the compactness of proteins (Fig. 3A and B). The RMSD plots showed that T41N/T150R system achieved equilibrium soon after the start of simulation, while the system was fluctuating for 15 ns before reaching equilibrium for the wild type. When the systems were equilibrium, it could be demonstrated by the slightly lower R_g values of the mutant that it had a closer conformation compared with the wild type, which might due to the hydrophilic effect of

T41N. During the last 2 ns, both systems were in equilibrium, and the average RMSF values for residues indicated that the stability of mutant could be due to the reduction of flexibility in the cap domain (Fig. 3C). There was no significant change around residue 41, however, as in Fig. 3D, T150R stabilized the cap domain by introducing salt bridges to the region with E154 and D164, which was coincident with our speculation. Accordingly, the results from MD simulations could explain why the mutations worked on the thermostability.

In conclusion, the residues at the active center could have positive effects on the enzymatic stability, and the thermostability of GthFAE was significantly enhanced by this strategy. The structure of GthFAE was determined in this study to support *in silico* strategies which not only significantly improved efficiency of wet experiments by rational design, but also assisted in elucidating the underlying mechanisms with molecular dynamics simulations. Despite the comparatively high thermostability of wild type, it could be even higher with the optimal temperature risen to 65 °C by the mutants. Moreover, T41N/T150R increased T_m to 80 °C (+6.4 °C) and exhibited a 35-fold $T_{1/2}$ at 70 °C by 201 min which could hardly be found in reported FAEs. This study is an initial step in the attempt to increase the industrial application of GthFAE that contributing to the paper manufacturing and further FA economic production.

Declaration of interest

The authors declare that they have no known competing financial interests or personal relationships that could have appeared to influence the work reported in this paper.

Acknowledgement

This work was supported by the Thousand Talents Program, China, Natural Science Foundation of Fujian Province (2019J01280 and 2021J01171), and Special Projects of the Central Government Guiding Local Science and Technology Development (2020L3008).

Appendix A. Supplementary data

Supplementary data to this article can be found online at https://doi.org/10.1016/j.bbrc.2022.02.074.

References

[1] D.M. Oliveira, T.R. Mota, B. Oliva, F. Segato, R. Marchiosi, O. Ferrarese-Filho, C.B. Faulds, W.D. Dos Santos, Feruloyl esterases: biocatalysts to overcome biomass recalcitrance and for the production of bioactive compounds, Bioresour. Technol. 278 (2019) 408–423.
[2] D.M. de Oliveira, A. Finger-Teixeira, T.R. Mota, V.H. Salvador, F.C. Moreira-Vilar, H.B. Molinari, R.A. Mitchell, R. Marchiosi, O. Ferrarese-Filho, W.D. dos Santos, Ferulic acid: a key component in grass lignocellulose recalcitrance to hydrolysis, Plant Biotechnol. J 13 (2015) 1224–1232.
[3] F. Ay Sal, D.N. Colak, H.I. Guler, S. Canakci, A.O. Belduz, Biochemical characterization of a novel thermostable feruloyl esterase from Geobacillus thermoglucosidasius DSM 2542(T), Mol. Biol. Rep. 46 (2019) 4385–4395.
[4] H. Zhang, B. Wen, Y. Liu, G. Du, X. Wei, K. Imam, H. Zhou, S. Fan, F. Wang, Y. Wang, F. Xin, A reverse catalytic triad Asp containing loop shaping a wide substrate binding pocket of a feruloyl esterase from Lactobacillus plantarum, Int. J. Biol. Macromol. 184 (2021) 92–100.
[5] G.M. Latha, P. Srinivas, G. Muralikrishna, Purification and characterization of ferulic acid esterase from malted finger millet (Eleusine coracana, Indaf-15), J. Agric. Food Chem. 55 (2007) 9704–9712.
[6] M.F. Andreasen, P.A. Kroon, G. Williamson, M.T. Garcia-Conesa, Esterase activity able to hydrolyze dietary antioxidant hydroxycinnamates is distributed along the intestine of mammals, J. Agric. Food Chem. 49 (2001) 5679–5684.
[7] C.B. Faulds, G. Williamson, The purification and characterization of 4-hydroxy-3-methoxycinnamic (ferulic) acid esterase from Streptomyces olivochromogenes, J. Gen. Microbiol. 137 (1991) 2339–2345.
[8] F.J. Contesini, R.R. Melo, H.H. Sato, An overview of Bacillus proteases: from production to application, Crit. Rev. Biotechnol. 38 (2018) 321–334.
[9] Z. Xu, Y.K. Cen, S.P. Zou, Y.P. Xue, Y.G. Zheng, Recent advances in the improvement of enzyme thermostability by structure modification, Crit. Rev. Biotechnol. 40 (2020) 83–98.
[10] L. Dai, Z. Chang, J. Yang, W. Liu, Y. Yang, C.C. Chen, L. Zhang, J.W. Huang, Y. Sun, R.T. Guo, Structural investigation of a thermostable-1,2-beta-mannobiose phosphorylase from Thermoanaerobacter sp. X-514, Biochem. Biophys. Res. Commun. 579 (2021) 54–61.
[11] T.R. Moharana, B. Pal, N.M. Rao, X-ray structure and characterization of a thermostable lipase from Geobacillus thermoleovorans, Biochem. Biophys. Res. Commun. 508 (2019) 145–151.
[12] X. Wang, J. Du, B. Zhao, H. Wang, S. Rao, G. Du, J. Zhou, J. Chen, S. Liu, Significantly improving the thermostability and catalytic efficiency of streptomyces mobaraenesis Transglutaminase through combined rational design, J. Agric. Food Chem. 69 (2021) 15268–15278.
[13] F.S. Aalbers, M.J. Furst, S. Rovida, M. Trajkovic, J.R. Gomez Castellanos, S. Bartsch, A. Vogel, A. Mattevi, M.W. Fraaije, Approaching boiling point stability of an alcohol dehydrogenase through computationally-guided enzyme engineering, Elife 9 (2020).
[14] L. Huang, J. Ma, J. Sang, N. Wang, S. Wang, C. Wang, H. Kang, F. Liu, F. Lu, Y. Liu, Enhancing the thermostability of phospholipase D from Streptomyces halstedii by directed evolution and elucidating the mechanism of a key amino acid residue using molecular dynamics simulation, Int. J. Biol. Macromol. 164 (2020) 3065–3074.
[15] Y. Suzuki, T. Kishigami, K. Inoue, Y. Mizoguchi, N. Eto, M. Takagi, S. Abe, Bacillus thermoglucosidasius sp. nov., a New species of Obligately thermophilic Bacilli, Syst. Appl. Microbiol. 4 (1983) 487–495.
[16] C.H. Zhu, Y.Y. Chen, M.N. Isupov, J.A. Littlechild, L.F. Sun, X.D. Liu, Q.C. Wang, H. Gong, P.P. Dong, N. Zhang, Y.K. Wu, Structural insights into a novel esterase from the East Pacific Rise and its improved thermostability by a semirational design, J. Agric. Food Chem. 69 (2021) 1079–1090.
[17] W. Minor, M. Cymborowski, D. Borek, D.R. Cooper, M. Chruszcz, Z. Otwinowski, Optimal structure determination from sub-optimal diffraction data, Protein Sci. 31 (2022) 259–268.
[18] A.J. McCoy, R.W. Grosse-Kunstleve, P.D. Adams, M.D. Winn, L.C. Storoni, R.J. Read, Phaser crystallographic software, J. Appl. Crystallogr. 40 (2007) 658–674.
[19] K.K. Lai, P.J. Stogios, C. Vu, X. Xu, H. Cui, S. Molloy, A. Savchenko, A. Yakunin, C.F. Gonzalez, An inserted alpha/beta subdomain shapes the catalytic pocket of Lactobacillus johnsonii cinnamoyl esterase, PLoS One 6 (2011), e23269.
[20] P. Emsley, B. Lohkamp, W.G. Scott, K. Cowtan, Features and development of Coot, Acta Crystallogr D Biol Crystallogr 66 (2010) 486–501.
[21] P.D. Adams, P.V. Afonine, G. Bunkoczi, V.B. Chen, I.W. Davis, N. Echols, J.J. Headd, L.W. Hung, G.J. Kapral, R.W. Grosse-Kunstleve, A.J. McCoy, N.W. Moriarty, R. Oeffner, R.J. Read, D.C. Richardson, J.S. Richardson, T.C. Terwilliger, P.H. Zwart, PHENIX: a comprehensive Python-based system for macromolecular structure solution, Acta Crystallogr D Biol Crystallogr 66 (2010) 213–221.
[22] G.M. Morris, R. Huey, W. Lindstrom, M.F. Sanner, R.K. Belew, D.S. Goodsell, A.J. Olson, AutoDock4 and AutoDockTools4: automated docking with selective receptor flexibility, J. Comput. Chem. 30 (2009) 2785–2791.
[23] M.T. Reetz, J.D. Carballeira, Iterative saturation mutagenesis (ISM) for rapid directed evolution of functional enzymes, Nat. Protoc. 2 (2007) 891–903.
[24] J. Schymkowitz, J. Borg, F. Stricher, R. Nys, F. Rousseau, L. Serrano, The FoldX web server: an online force field, Nucleic Acids Res. 33 (2005) W382–W388.
[25] L. Holm, Using dali for protein structure comparison, Methods Mol. Biol. 2112 (2020) 29–42.
[26] K.K. Lai, G.L. Lorca, C.F. Gonzalez, Biochemical properties of two cinnamoyl esterases purified from a Lactobacillus johnsonii strain isolated from stool samples of diabetes-resistant rats, Appl. Environ. Microbiol. 75 (2009) 5018–5024.
[27] X.F. Zhang, G.Y. Yang, Y. Zhang, Y. Xie, S.G. Withers, Y. Feng, A general and efficient strategy for generating the stable enzymes, Sci. Rep. 6 (2016) 33797.